Spatial characterization of doped SiC wafers by Raman spectroscopy

J. C. Burton, L. Sun, M. Pophristic, S. J. Lukacs, F. H. Long, Z. C. Feng, and I. T. Ferguson

Citation: Journal of Applied Physics **84**, 6268 (1998); doi: 10.1063/1.368947
View online: http://dx.doi.org/10.1063/1.368947
View Table of Contents: http://scitation.aip.org/content/aip/journal/jap/84/11?ver=pdfcov
Published by the AIP Publishing

Spatial characterization of doped SiC wafers by Raman spectroscopy

J. C. Burton, L. Sun, M. Pophristic, S. J. Lukacs, and F. H. Long[a)]
Department of Chemistry, Rutgers University, Piscataway, New Jersey 08854–8087

Z. C. Feng
Institute for Materials Research and Engineering, National University of Singapore, Singapore 119260

I. T. Ferguson
EMCORE Corporation, Somerset, New Jersey 08873

(Received 20 April 1998; accepted for publication 28 August 1998)

Raman spectroscopy has been used to investigate wafers of both 4H–SiC and 6H–SiC. The wafers studied were semi-insulating and *n*-type (nitrogen) doped with concentrations between 2.1×10^{18} and 1.2×10^{19} cm^{-3}. Significant coupling of the A_1 longitudinal optical (LO) phonon to the plasmon mode was observed. The position of this peak shows a direct correlation with the carrier concentration. Examination of the Raman spectra from different positions on the wafer yielded a rudimentary spatial map of the carrier concentration. These data are compared with a resistivity map of the wafer. These results suggest that Raman spectroscopy of the LO phonon–plasmon mode can be used as a noninvasive, *in situ* diagnostic for SiC wafer production and substrate evaluation. © *1998 American Institute of Physics.* [S0021-8979(98)03623-8]

I. INTRODUCTION

Silicon carbide (SiC) has recently been recognized as an important material for a wide variety of high-power and high-temperature electronic applications. SiC exhibits a large number (250) of polytypes with different structural and physical properties.[1] The polytypes have the same chemical composition but exhibit different crystallographic structures and stacking sequences along the principal crystal axis. Several important polytypes of SiC such as 4H and 6H have C_{6v} crystallographic symmetry. In the *a* direction 4H– and 6H–SiC are almost identical (<1% change); however, the 4H polytype consists of four units in the *c* direction and the 6H consists of six units. Different polytypes have different band gaps, electron mobilities, and other physical properties; for example, 4H–SiC has attracted significant attention due to its high electron mobility and excellent thermal properties. Recently high quality wafers of both 4H– and 6H–SiC have been grown.[2,3] Wafers of SiC are also a promising substrate for nitride semiconductor growth due to their compatible lattice structure and similar thermal expansion coefficients.

If the full potential of SiC is to be reached, highly uniformly doped SiC wafers must be produced. As is shown in this article, heavily doped SiC wafers are often not spatially uniform. Spatially inhomogeneous doping of the SiC substrate produces nonuniform thermal properties and subsequently poor quality epilayers. Common measurement techniques for electrical characterization such as Hall and resistivity require direct contact with the sample. Contact with the sample surface may prevent or impair the later growth of epilayers. A noncontact method for the spatial profiling of SiC wafers will provide a necessary quantitative technique for the solution of this problem.

[a)]Author to whom correspondence should be addressed; electronic mail: fhlong@rutchem.rutgers.edu

There have been several previous experimental studies of the one-phonon Raman spectra of SiC.[4–11] The importance of polytypes on the one-phonon Raman spectra of SiC was first noted by Choyke and collaborators.[4,5] Raman has been shown to be a valuable probe of SiC grown by a variety of techniques.[12,13]

In this study, we have performed Raman scattering measurements at room temperature for semi-insulating 4H–SiC and heavily doped 4H–SiC and 6H–SiC wafers. The doped wafers of SiC were *n* type, nitrogen doped, with concentrations ranging from 2.1×10^{18} to 1.2×10^{19} cm^{-3}. A semi-insulating wafer of 4H–SiC was also examined as a reference. Nitrogen is well established as a donor in SiC.[1,14] Significant changes were observed in the shape and position of the A_1 longitudinal optical (LO) phonon as a function of doping concentration. The changes in peak position, spectral shape, and width of the A_1(LO) phonon are attributed to plasmon–phonon coupling. The experimental Raman line shape was compared with theory.[15]

We have exploited the plasmon–phonon coupling to estimate the spatial dependence of the carrier concentration across the SiC wafer. Unlike electrical conductivity measurements, which involve the attachment of an electrical contact to the material, Raman spectroscopic determination of carrier concentrations is nondestructive and noncontact. The spatial resolution of the Raman scattering is determined by the spot size of the laser, which can be as small as 1 μm in diameter. The spatial characterization of SiC wafers is important if these materials are to be used in high-power electronics or as a substrate for nitride semiconductor growth.

II. EXPERIMENT

Raman spectra were recorded using a Coherent Model INNOVA 90 Ar/Kr laser, a SPEX Model 1877E triple monochromator, and a charge-coupled detector (CCD) cooled with

liquid nitrogen. The samples analyzed were held in a rotary mount at room temperature. The samples were aligned such that the collection of scattered light was in the near backscattered geometry perpendicular to the (0001) face of the sample, so that the same spot on each sample could be excited at each different laser wavelength. Raman spectra were taken at several different spots on each wafer to gauge the homogeneity of the doping in each wafer. The polarization of the laser light, both incident and collected, was unspecified. Calibration of each Raman spectrum was carried out using known atomic emission lamps and is accurate to approximately 0.5 cm^{-1}. Typically 10 min scans were used to acquire the Raman data.

A series of both 4H– and 6H–SiC wafers from a variety of sources were examined. The wafers used were up to 2 in. in diameter. All the doped wafers studied were *n*-type nitrogen doped. The 4H–SiC wafers were cut 8° off axis. The 6H wafers were cut at either 3.5° or 0° off axis. The resistivity map was made using equipment from Lehighton Electronics Inc. The head size used was 0.56 in. in diameter.

III. RESULTS AND DISCUSSION

A. Raman spectra

Group-theoretical analysis shows that the Raman-active modes of a wurtzite structure, which has C_{6v} symmetry, are the A_1, E_1, and E_2 modes.[16] The A_1 and E_1 phonon modes, which are also infraed (IR) active, are split into LO and transverse optical (TO) modes. In a backscattering geometry, where the incident and collected light are parallel to the *c* axis of the sample, the A_1(LO), E_1(TO), and E_2 phonons are expected to be seen in the Raman spectra at excitation energies which are nonresonant.[16,17] Since the band gap of hexagonal SiC is approximately 3.3 eV for 4H–SiC and 3.0 eV for 6H–SiC[1] and our excitation energy is no greater than 2.6 eV, the nonresonant selection rules are appropriate. We note that the 4H–SiC wafers studied were cut 8° off the *c* axis; however this is too small to significantly change the Raman selection rules.

As noted earlier, the existence of SiC polytypes has a major impact on the Raman spectra.[13] The one-phonon Raman spectra of 6H–, 4H–, and other polytypes of SiC can be explained by the folding of the Brillouin zone due to the polytype behavior of SiC.[4,5] Because different SiC polytypes only differ by the length of the *c* axis, only the Brillouin zone in the direction of Γ-L is effected. This folding makes modes away from the Γ point visible in the one-phonon Raman spectrum. Group theory can be used to identify the symmetry of these additional modes. Phonons with atomic motion parallel to the *c* axis are designated axial and phonons perpendicular to the *c* axis are planar.

In Fig. 1(a) and 1(b) we show typical Raman data for 4H–SiC, taken at room temperature. Figures 2(a) and 2(b) show data taken under the same conditions for 6H–SiC. The major peaks in the 4H–SiC Raman spectra are identifiable from previous studies.[4,5] The peak at 203.5 cm^{-1} is an E_2 planar or transverse acoustic (TA) mode, 610.5 cm^{-1} is A_1 axial or longitudinal acoustic (LA), 777.0 cm^{-1} is E_2 planar optical, 797.5 cm^{-1} is an E_1 mode, and 967.0 cm^{-1} is

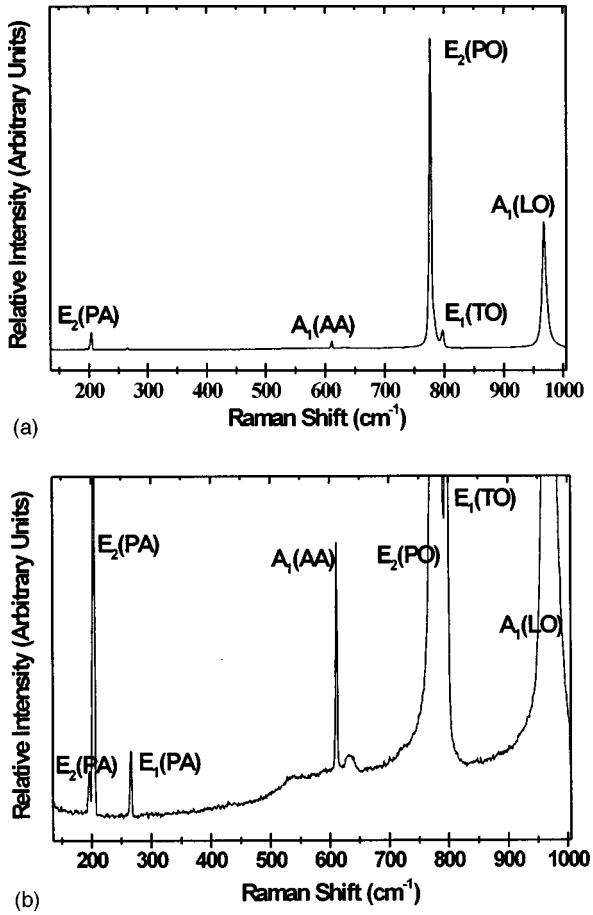

FIG. 1. (a) Raman spectrum of 4H–SiC wafer taken with 514.5 nm laser light at room temperature (nominal nitrogen concentration=2.1×10^{18} cm^{-3}). The strongest peaks are E_2(TA), 203.5 cm^{-1}; E_2(TO), 610.5 cm^{-1}; E_2(TO), 777.0 cm^{-1}; E_1(TO), 797.5 cm^{-1}; A_1(LO) 967.0 cm^{-1}. (b). Same data as (a) but with an expanded *y* scale.

A_1(LO). The primary peaks in 6H–SiC are an E_2 planar acoustic mode at 150.5 cm^{-1}, two planar or TO modes of E_2 symmetry at 767.5 and 788.0 cm^{-1}, and an A_1(LO) phonon at 966.5 cm^{-1}. The mode at 796.0 cm^{-1} is a planar optical mode of E_1 symmetry. We note that with different experimental arrangements, different symmetry modes may be seen. For example, A_1 and E_1 modes may cause a peak at approximately 788 cm^{-1} in the 6H–SiC spectrum in addition to, or instead of, the E_2 mode to which we have assigned that peak, depending on experimental geometry.[4,5]

The high quality of the data obtained in our experiments allows for the observation of several weaker peaks present in the Raman spectra. These additional peaks, with symmetry identification, are also listed in Table I. In the 4H–SiC Raman spectra, two small additional features are worth noting. A pedestal is seen in the 4H–SiC Raman spectra, starting around 500 cm^{-1}. This pedestal appears at the same location in the Raman spectra as the laser wavelength is varied; therefore we conclude that this feature is Raman scattering and not luminescence. A similar feature is also seen in the 6H–SiC Raman spectrum. The Si–Si bond appears at approximately 519 cm^{-1};[18] however, the feature in our experiments is sufficiently broad that we believe that this explanation is unlikely. We have attributed this feature to the acoustic

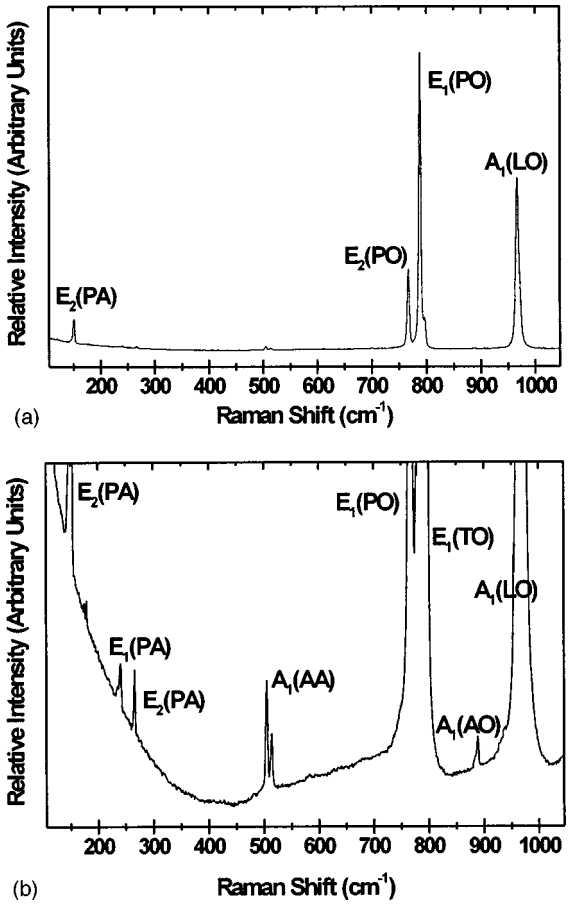

FIG. 2. (a) Raman spectrum of 6H–SiC wafer taken with 514.5 nm laser light at room temperature (nominal nitrogen concentration $=2.1\times10^{18}$ cm^{-3}). The strongest peaks are E_2(TA), 150.5 cm^{-1}; E_2(TO), 767.5 cm^{-1}; E_1(TO), 788.0 cm^{-1}; A_1(LO), 966.5 cm^{-1}. (b) Same data as (a) but with an expanded *y* scale.

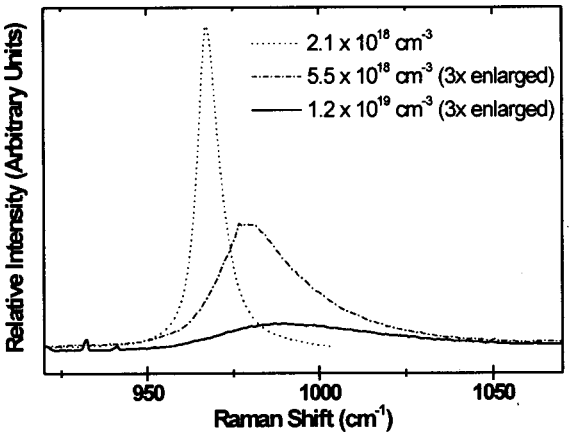

FIG. 3. High frequency optical phonon A_1(LO) in 4H–SiC at several nitrogen concentrations. The dotted line is 2.1×10^{18} cm^{-3}; dot-dash line 5.5×10^{18} cm^{-3}; solid line 1.2×10^{19} cm^{-3}. Experimental conditions as in Figs. 1 and 2. The A_1(LO) phonon increases in frequency and broadens with increasing doping and carrier concentration.

branch of the second-order Raman spectra. Theoretical calculations support this assignment.[19,20] The experimental second-order Raman spectra of 4H– and 6H–SiC will be discussed in another article.[21]

Around 630 cm^{-1} another feature is clearly seen. In many samples, this feature appears as a doublet. Variation of the laser wavelength has also verified that this peak is due to Raman scattering. Because the amplitude of this peak does not significantly change with nitrogen doping concentration, and is still observed in the Raman spectrum of the semi-insulating sample, we discount the possibility that this peak is due to a local mode of the nitrogen dopant atom. This peak is the subject of further investigation.

Two peaks at around 500 cm^{-1} are visible in the 6H–SiC Raman spectra, shown in Fig. 2(b). In addition, there appears to be a broad peak underneath the two sharper features. The two peaks at 505 and 513 cm^{-1} are A_1 LA modes associated with the $q=0.67$ point ($q=k/k_{max}$) of the reduced Brillouin zone. The broad background signal increases in magnitude and sharpens when the sample is cooled to 77 K. This behavior is consistent with the assignment of this feature by Klein and co-workers as Raman scattering from electronic defects.[6]

In Fig. 3 we show the A_1(LO) phonon line shape as a function of nitrogen doping concentration. As the doping concentration is increased, the phonon increases in frequency and asymmetrically broadens. The change in nitrogen concentration from 2.1×10^{18} to 1.2×10^{19} cm^{-3} in 4H–SiC produces a dramatic change in the position and shape of the A_1(LO) phonon. This large change in the frequency of the A_1(LO) phonon makes its position a sensitive probe of doping in this concentration range. We note that none of the other strong Raman peaks shift or broaden in the doping concentration range studied.

TABLE I. Peak assignment for peaks shown in Figs. 1 and 2.

4H–SiC peak Raman shift (cm^{-1})	Mode symmetry	6H–SiC peak Raman shift (cm^{-1})	Mode symmetry
195.5	E_2 planar acoustic	146.0, 150.5	E_2 planar acoustic
203.5	E_2 planar acoustic	235.0, 240.0	E_1 planar acoustic
266.0	E_1 planar acoustic	266.0	E_2 planar acoustic
610.5	A_1 axial acoustic	505.0, 513.5	A_1 axial acoustic
777.0	E_2 planar optic	767.5, 788.0	E_2 planar optic
797.5	E_1(TO)	796.0	E_1(TO)
		888.5	A_1 axial optic
967.0	A_1(LO)	966.5	A_1(LO)

B. Comparison of A_1(LO) phonon line shape with theory

The behavior of the A_1(LO) phonon can clearly be attributed to plasmon–phonon coupling. The strong dependence of the A_1(LO) peak position on carrier concentration allows us to use the position of the A_1(LO) phonon as a measure of the carrier concentration. Previous studies have used this approach to examine other wide gap materials such as GaN at high doping concentrations.[22]

Physically, at sufficiently large carrier concentration, longitudinal oscillations of the associated plasma modify the dielectric constant and consequently the Raman cross section. Klein and collaborators developed the first theory for the effects of plasmon–phonon coupling on Raman line shapes.[6] This theory has been refined by other research groups. For example, Irmer *et al.* extended the theory to include phonon dampening.[15] These works have established that in wide band gap semiconductors the dominant mechanisms for Raman scattering are electro-optical and deformation potential, and not fluctuations in carrier density. The line shape of the LO phonon is given by

$$I(\omega)=SA(\omega)\mathrm{Im}[-1/\epsilon(\omega)], \tag{1}$$

where

$$A(\omega)=1+2C\omega_T^2[\omega_p^2\gamma(\omega_T^2-\omega^2)-\omega^2\Gamma(\omega^2-\gamma^2-\omega_p^2)/\Delta+(C^2\omega_T^4/\Delta)\{\omega_p^2[\gamma(\omega_l^2-\omega_T^2)+\Gamma(\omega_p^2-2\omega^2)+\omega^2\Gamma(\omega^2+\gamma^2)\}/(\omega_l^2-\omega_T^2), \tag{2}$$

and

$$\Delta=\omega_p^2\gamma[(\omega_T^2-\omega^2)^2+(\omega\Gamma)^2]+\omega^2\Gamma(\omega_l^2-\omega_T^2)\times(\omega^2+\gamma^2), \tag{3}$$

ω_l and ω_T are the longitudinal and transverse optical phonon frequencies, γ is the plasmon dampening constant, Γ is the phonon dampening constant, and C is the Faust–Henry coefficient. S is a proportionality factor. The dielectric function $\epsilon(\omega)$ contains a phonon and a plasmon contribution:

$$\epsilon(\omega)=\epsilon_\infty\left(1+\frac{\omega_l^2-\omega_T^2}{\omega_T^2-\omega^2-i\omega\Gamma}-\frac{\omega_p^2}{\omega(\omega+i\gamma)}\right), \tag{4}$$

where ω_p, the plasma frequency, is given in cgs units by

$$\omega_p^2=\frac{ne^2 4\pi}{m_{eff}\epsilon_\infty}. \tag{5}$$

This model has been previously used to examine plasmon–phonon coupling in SiC[10,12] and other wide band semiconductors.[23]

We have used a commercial graphing program to fit our data. Using Eqs. (1)–(4), we fixed ω_T, ω_L, and C to accepted literature values ($C=0.43$; $\omega_T=783\ \mathrm{cm}^{-1}$; $\omega_L=965\ \mathrm{cm}^{-1}$).[10] The value for ω_L was confirmed by our own measurements of semi-insulating 4H–SiC (964.5 cm^{-1}). We then allowed the program to find the values for Γ, γ, and ω_p that gave the best agreement between the fit and the experimental line shape. We were then able to relate these values to the nominal doping concentrations of each wafer, which enables us to make an estimate of nominal doping level for any given value of ω_p. The quality of the theoretical fits to the data is good. Typical results for 4H–SiC are shown in Fig. 4. We have found that the high frequency tail of the A_1(LO) phonon can be reproduced in this manner. Minor deviations from the theory may be due to a background signal from second-order Raman scattering of the acoustic phonons. Similar quality fits are found for the 6H–SiC.

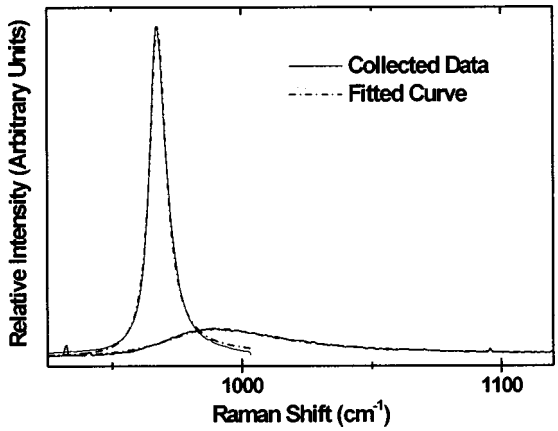

FIG. 4. Comparison of A_1(LO) phonon line shape with theory. The plasma frequency was found by fitting the line shapes to the equations. The collected data is a solid line. The fitted curve is a dot-dashed line. Nominally the nitrogen concentrations are 2.1×10^{18} and $1.2\times10^{19}\ \mathrm{cm}^{-3}$. (For $2.1\times10^{18}\ \mathrm{cm}^{-3}$: $\Gamma=4.43\ \mathrm{cm}^{-1}$, $\gamma=436\ \mathrm{cm}^{-1}$, and $\omega_p=154\ \mathrm{cm}^{-1}$.) (For $1.2\times10^{19}\ \mathrm{cm}^{-3}$: $\Gamma=25.1\ \mathrm{cm}^{-1}$, $\gamma=593\ \mathrm{cm}^{-1}$, and $\omega_p=383\ \mathrm{cm}^{-1}$.)

In Fig. 5 we plot the A_1(LO) phonon peak position measured at the center of each wafer versus the nominal nitrogen concentration for different 4H–SiC wafers. A clear correspondence is observed. Therefore, we can use the position of the A_1(LO) phonon to empirically estimate the carrier concentration. This trend can be explained by considering the expression for the high frequency coupled plasmon–phonon mode in the limit of no dampening.

$$(\omega^+)^2=\tfrac{1}{2}\{\omega_l^2+\omega_p^2+[(\omega_l^2+\omega_p^2)^2-4\omega_p^2\omega_T^2]^{1/2}\}, \tag{6}$$

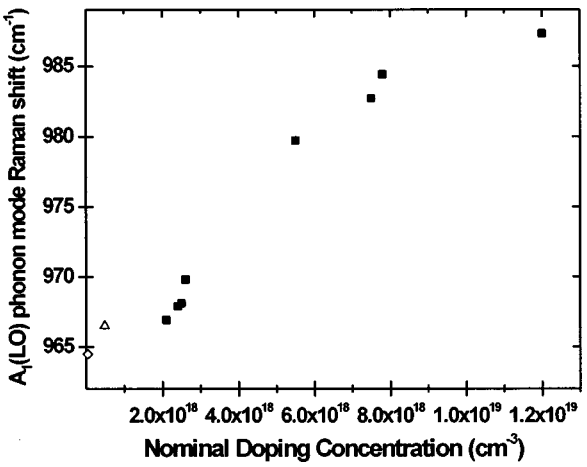

FIG. 5. Average A_1(LO) phonon position vs nominal nitrogen concentration. Filled squares show our data; the open diamond shows A_1(LO) phonon frequency for semiinsulating 4H–SiC as reference; and the open triangle shows estimated Raman shift from Ref. 10.

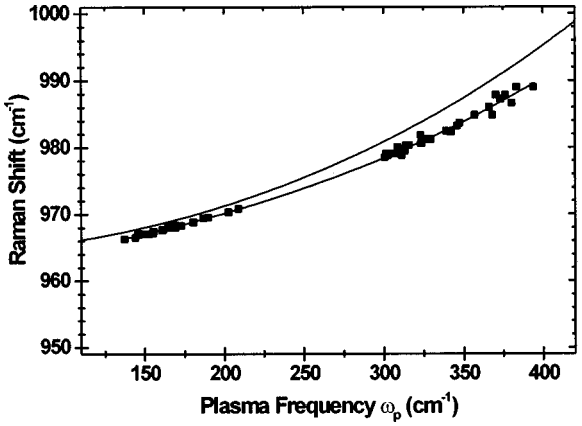

FIG. 6. A_1(LO) phonon position vs plasma frequency obtained from fits. Solid squares are experimental values; the line through the experimental data is shown to guide the eye. The line above the data is the prediction of Eq. (6).

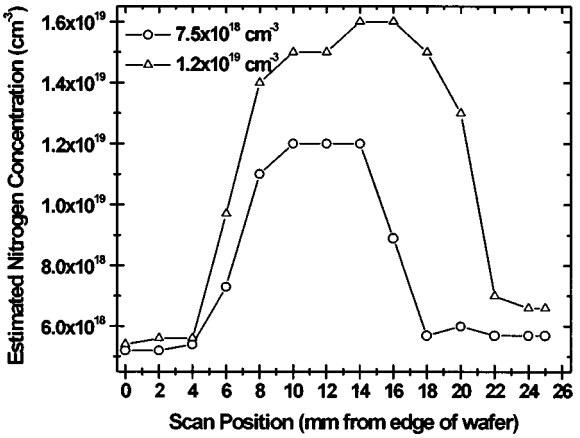

FIG. 8. Estimated carrier concentration profile along two heavily doped 4H–SiC wafers as determined by Raman spectroscopy with nominal nitrogen concentrations noted in the legend.

where ω_l, ω_p, and ω_T are defined as above. A plot of the measured A_1(LO) phonon peak positions versus the plasma frequencies obtained from the fits is shown in Fig. 6. This figure shows all data from spectra taken at different positions on each wafer. A line is drawn through the data to guide the reader. A comparison with Eq. (6) is also shown. The deviation between Eq. (6) and the experimental data is larger for increased plasma frequency due to the neglect of plasmon damping. The plasma frequency determines the position of the A_1(LO) phonon and the Faust–Henry coefficient and the two damping parameters control the width and asymmetry of the peak.

C. Spatial characterization of SiC wafers

To address the need for noncontact, *in situ* diagnostics for SiC wafers we have examined the spatial dependence of the Raman scattering from the A_1(LO) phonon. In Fig. 7 and 8 we show typical results for the spatial dependence of the doping level in SiC wafers, as determined by Raman spectroscopy. Figure 7 is the A_1(LO) phonon frequency across the wafer. Figure 8 shows the nitrogen concentration which we have estimated from the A_1(LO) phonon frequency across the wafer. We note that the spatial dependence is not the same for each SiC wafer and that the concentration profile is often not symmetric with respect to rotations of the wafer. The high carrier concentration observed in the center of the wafer corresponds to a dark spot visually observed in the high nitrogen concentration wafers. The far edges of both wafers had doping levels estimated to be much lower than the nominal value specified for the wafer.

A resistivity map for a doped SiC wafer is shown in Fig. 9. The resistivity map confirms the spatial nonuniformity of the doping concentration. In the most heavily doped 4H–SiC wafer, the resistivity varied by 20.2%. This is consistent with the noncontact Raman measurements on the same wafer, where a variation of approximately 26% was observed over a similar portion of the center of the wafer. The lowest resistivity point in the 4H–SiC wafer occurs near the geometric center of the wafer. This is also consistent with Raman measurements, which demonstrated that the carrier concentration was highest near the center of the wafer. Furthermore, as was found in the Raman measurements, the lower doped wafers

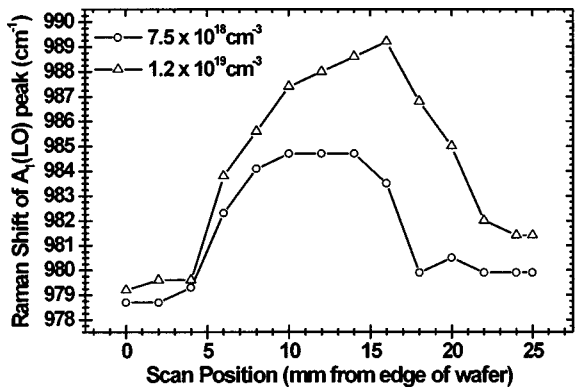

FIG. 7. Spatial profile of the A_1(LO) phonon energy across two 4H–SiC wafers with nominal nitrogen concentrations noted in the legend.

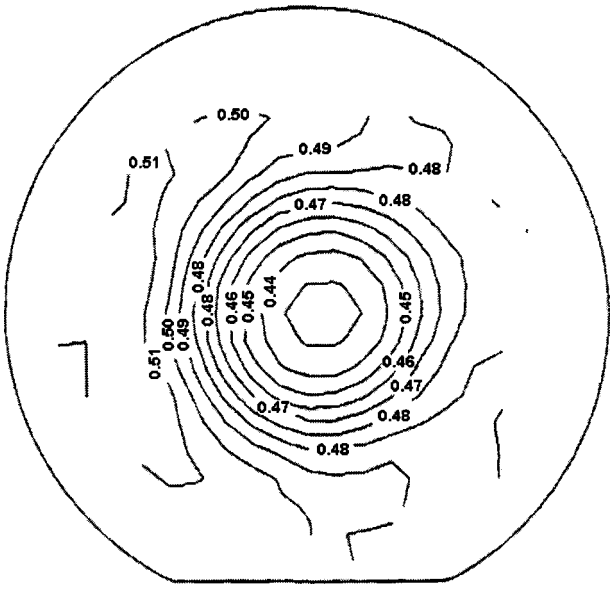

FIG. 9. Resistivity map for the 4H–SiC wafer nominally doped at 1.2 $\times 10^{19}$ cm^{-3}.

were more spatially uniform with respect to doping concentration. In order to correlate the Raman and resistivity data more quantitatively, accurate mobility data are needed. The data in Figs. 6 and 7 correspond to a horizontal scan from right to left through the center of the wafer, which is oriented as shown in Fig. 9.

The results suggest that Raman spectroscopy can be used as an *in situ* probe of the spatial dependence of the carrier concentration for SiC wafers. Other methods for the determination of carrier concentration such as Hall or resistivity measurements involve the direct contact of the sample with electrodes. Photoluminescence can be used to measure the nitrogen concentration in SiC at concentrations between 10^{14} and 10^{17} cm^{-3}; however these measurements require cryogenic temperatures.[24]

In a recent report, Galeckas *et al.* have examined the spatial dependence of the free carrier absorption and lifetime in 4H–SiC epilayers.[25] A significant spatial variation was observed in the free carrier lifetime. The substrates used in this study were similar to the high concentration sample in our study. The large spatial variation observed in the doping level might be partially responsible for the observations of Galeckas *et al.*[25] Further work in this direction is planned.

IV. CONCLUSIONS

We have used Raman spectroscopy to investigate wafers of 4H– and 6H–SiC. Theoretical models of plasmon–phonon coupling successfully predict the experimental A_1(LO) phonon line shape at dopant concentrations up to 10^{19} cm^{-3}. The phonon–plasmon coupling of the A_1(LO) phonon can be used as a measure of carrier concentration. We have used the line shape of the A_1(LO) phonon to estimate the spatial dependence of the carrier concentration across the wafer. The results suggest that Raman scattering of the phonon can be used as an *in situ*, noncontact diagnostic of doping uniformity in semiconductor production. This is in contrast to electrical conductivity measurements, which require contact with the samples.

ACKNOWLEDGMENTS

Acknowledgment is made to the donors of the Petroleum Research Fund, administered by the ACS, for the partial support of this research. Additional support was provided by the Rutgers Research Council. One of the authors (F.H.L.) would like to thank the Coherent Corporation for the loan of the INNOVA 70 laser. One of the authors (Z.C.F.) acknowledges the support of Professor C. F. Shih and Professor S. J. Chua. The authors would like to thank Dr. A. Ermakov for useful discussions. They would also like to thank Paul Cooke of EMCORE Corporation for the resistivity maps.

[1] W. J. Choyke and G. Pensl, MRS Bull. **22**, 25 (1997).
[2] R. C. Glass, D. Henshall, V. F. Tsvetkov, and C. H. Carter, MRS Bull. **22**, 30 (1997).
[3] D. Hoffman, R. Eckstein, M. Kolbl, Y. Makarov, S. G. Muller, and E. Schmitt, J. Cryst. Growth **174**, 669 (1997).
[4] D. W. Feldman, J. H. Parker, Jr., W. J. Choyke, and L. Patrick, Phys. Rev. **170**, 698 (1968).
[5] D. W. Feldman, J. H. Parker, Jr., W. J. Choyke, and L. Patrick, Phys. Rev. **173**, 787 (1968).
[6] M. V. Klein, B. N. Ganguly, and P. J. Colwell, Phys. Rev. B **6**, 2380 (1972).
[7] D. Olego and M. Cardona, Phys. Rev. B **25**, 1151 (1982).
[8] H. Yugami, S. Nakashima, A. Mitsuishi, A. Uemoto, M. Shigeta, K. Furukawa, A. Suzuki, and S. Nakajima, J. Appl. Phys. **61**, 354 (1987).
[9] Z. C. Feng, A. J. Mascarenhas, W. J. Choyke, and J. A. Powell, J. Appl. Phys. **64**, 3176 (1988).
[10] H. Harima, S.-I. Nakashima, and T. Uemura, J. Appl. Phys. **78**, 1996 (1995).
[11] Z. C. Feng, A. Rohatgi, C. C. Tin, R. Hu, A. T. S. Wee, and K. P. Se, J. Electron. Mater. **25**, 917 (1996).
[12] H. Okumura, E. Sakuma, J. H. Lee, H. Mukaida, S. Misawa, K. Endo, and S. Yoshida, J. Appl. Phys. **61**, 1134 (1987).
[13] S. Nakashima and H. Harima, Phys. Status Solidi A **162**, 37 (1997).
[14] W. Suttrop, G. Pensl, W. J. Choyke, R. Stein, and S. Leibenzender, J. Appl. Phys. **72**, 3708 (1992).
[15] G. Irmer, V. V. Toporov, B. H. Bairamov, and J. Monecke, Phys. Status Solidi A **119**, 595 (1983).
[16] W. Hayes and R. Loudon, *Scattering of Light by Crystals*, 1st ed. (Wiley, New York, 1978).
[17] *Light Scattering In Solids II*, edited by M. Cardona and G. Guntherodt (Springer, New York, 1982), Vol. 50.
[18] P. Y. Yu and M. Cardona, *Fundamentals of Semiconductors* (Springer, New York, 1996).
[19] W. Windl, K. Karch, P. Pavone, O. Schutt, D. Strauch, W. H. Weber, K. C. Hass, and L. Rimai, Phys. Rev. B **49**, 8764 (1994).
[20] A. Zywietz, K. Karch, and F. Bechstedt, Phys. Rev. B **54**, 1791 (1996).
[21] J. C. Burton, L. Sun, F. H. Long, Z. C. Feng, and I. T. Ferguson, Phys. Rev. B. (submitted).
[22] P. Perlin, C. Jauberthie-Carillon, J.-P. Itie, A. S. Miguel, I. Grzegory, and A. Polian, Phys. Rev. B **45**, 83 (1992).
[23] P. Perlin, J. Camassel, W. Knap, T. Taliercio, J. C. Chervin, T. Suski, I. Grzegory, and S. Porowski, Appl. Phys. Lett. **67**, 2524 (1995).
[24] I. G. Ivanov, C. Hallin, A. Henry, O. Kordina, and E. Janzen, J. Appl. Phys. **80**, 3504 (1996).
[25] A. Galeckas, V. Grivickas, J. Linnros, H. Bleichner, and C. Hallin, J. Appl. Phys. **81**, 3522 (1997).